THE JOURNAL OF PHYSICAL CHEMISTRY C

Article

Cite This: J. Phys. Chem. C 2019, 123, 23635−23642

pubs.acs.org/JPCC

Tunable Negative Permittivity in Flexible Graphene/PDMS Metacomposites

Kai Sun,[†] Jiannan Dong,[†] Zongxiang Wang,[†] Zhongyang Wang,[‡,§] Guohua Fan,[‡] Qing Hou,[*,∥] Liqiong An,[†] Mengyao Dong,[⊥] Runhua Fan,[*,†] and Zhanhu Guo[*,#]

[†]College of Ocean Science and Engineering, Shanghai Maritime University, Shanghai 201306, China

[‡]School of Materials Science and Engineering, Shandong University, Jinan 250061, China

[§]Department of Materials Science and Engineering, Faculty of Engineering, National University of Singapore, Singapore 119077, Singapore

[∥]Kathleen Lonsdale Materials Chemistry, Department of Chemistry, University College London, London WC1H 0AJ, U.K.

[⊥]National Engineering Research Center for Advanced Polymer Processing Technology, Zhengzhou University, Zhengzhou 450002, China

[#]Integrated Composites Laboratory (ICL), Department of Chemical & Biomolecular Engineering, University of Tennessee, Knoxville, Tennessee 37996, United States

ABSTRACT: The flexible metacomposites with tunable negative permittivity have great potential in wearable cloaks, stretchable sensors, and thin-film capacitors, etc. In this paper, the flexible graphene/polydimethylsiloxane (GR/PDMS) metacomposites with tunable negative permittivity were prepared by an in situ polymerization method. The ac conductivity behavior, dielectric property, and impedance performance of the resulting composites with different graphene mass ratios (0−4 wt %) were studied. With the increase of graphene, the conductive mechanism of the resulting composites changed from hopping conduction to electron conduction, along with the change of microstructure. When graphene content in the composites came up to 3 wt %, the negative permittivity conforming to Drude model was observed. Further investigation revealed that there is a corresponding relationship between the permittivity and the reactance. It is demonstrated that the inductive character is responsible for the negative permittivity, while the capacitive character results in the positive permittivity.

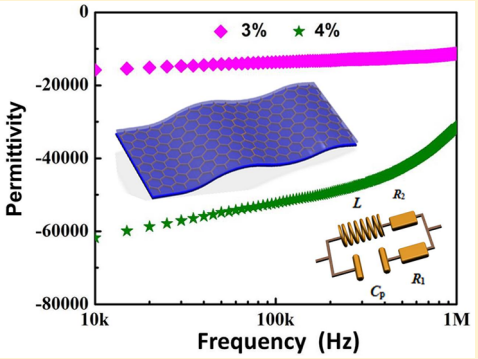

1. INTRODUCTION

When it comes to dielectric constant, it traditionally means positive permittivity, which describes the interaction of a material with an electric field. In recent years, the materials with negative permittivity (i.e., the ε-negative materials) have been a research hotspot, owing to their great potential applications in negative capacitance field effect transistors,[1] coil-free resonators,[2] novel capacitors,[3] and high-power microwave filters,[4] etc.

Actually, the negative permittivity behavior has triggered considerable interest since the appearance of the electromagnetic metamaterials,[5−7] which are made of periodically structural units. As compared with the conventional materials, the properties of electromagnetic metamaterials are mainly dependent on their periodic structures including shape, size, and orientation of the units rather than on their intrinsic compositions and microstructures.[8] As a supplement and extension for the artificially electromagnetic metamaterials, the "real" materials with negative permittivity fabricated by a versatile and universal technique in materials field have aroused in the researcher a wide range of interest.[9−11] These ε-negative materials are termed as intrinsic metamaterials or metacomposites,[12] which can facilely and effectively achieve their tunable properties by adjusting their compositions and microstructures. Additionally, metacomposites possess an isotropic electromagnetic response owing to their homogeneous structure.[13] Hence, metacomposites have become a burgeoning research focus in recent years.[14−18]

Definitely, the negative permittivity was early observed in metals derived from the plasma oscillation of electrons,[19] but the absolute values of negative permittivity are too gigantic in radio frequency due to the ultrahigh electron density in metals. Meanwhile, the loss of metals is more tremendous than the permittivity, leading to the fact that the complex permittivity is approximately an imaginary value in radio frequency. The strong negative permittivity and huge dissipation are unexpected for metal materials' applications and performance, such as impedance mismatching.[20] In fact, the weakly negative permittivity with a small absolute value can be applied to novel capacitors with high permittivity and perfect absorption.[21,22]

Received: July 16, 2019
Revised: August 22, 2019
Published: August 22, 2019

DOI: 10.1021/acs.jpcc.9b06753
J. Phys. Chem. C 2019, 123, 23635−23642

For instance, Shi et al.[23] have designed a bilayer structure composed of a weakly negative permittivity and a positive permittivity to obtain a novel capacitor with high permittivity and low dissipation. To overcome the obstacles of the strongly negative permittivity in practical applications, there is an urgent requirement in reducing the plasma frequency of metals to microwave frequency region. In our previous investigations, the metal particles (such as Ni,[24] Fe,[25] Ag,[26] Cu,[27] and alloys[28]) were embedded into the insulating ceramic matrix to dilute the electron density, and a low frequency plasmonic state was observed. Afterward, the polymer-based metacomposites with metal particles or conductive polymers have also been fabricated and realized the negative permittivity.[29−32]

It is suggested that the negative permittivity and the plasma frequency are closely related to the free carrier density of the conductive fillers.[33] Compared with that of metal and conductive polymers, carbon materials possess moderate electron density and can be a preferable substitute for negative permittivity.[34] As a novel two-dimensional carbon material, graphene can become a promising candidate to realize the negative permittivity due to their unique electrical property.[35] In fact, it is feasible to achieve negative permittivity behavior in ceramic-based composites by taking advantage of graphene.[18,36]

Compared to the ceramic-based metacomposites with negative permittivity, the polymer-based metacomposites endowed with excellent flexibility have an overwhelming advantage in processing and application especially in flexible electronic devices, wearable cloaks,[37] stretchable sensors,[38] and thin-film capacitors.[39] Therefore, this paper is devoted to the study of flexible metacomposites with tunable negative permittivity. Interestingly, graphene, the desirable candidate for negative permittivity, can also be widely used in the flexible electronic devices owing to their excellent conductivity, high carrier mobility, and good mechanical flexibility.[40] As a result, graphene was chosen as the functional composition. Furthermore, it is worth noting that an appropriate substrate plays a significant role in the flexible metacomposites. Currently, thermoplastic elastomer, polyurethane, and silicone rubber can be regarded as a flexible substrate.[41−43] As a typical representative of silicone rubber, polydimethylsiloxane (PDMS) is a suitable hosting matrix for the flexible, wearable, and stretchable devices, due to its outstanding elasticity, deformation resistance, nonflammability, biological compatibility, high weatherability, and convenient preparation.[44]

In this paper, we proposed to choose PDMS and conductive graphene as the matrix and functional fillers to fabricate the flexible GR/PDMS metacomposites by an in situ polymerization process. In addition, their conductivity behavior, dielectric properties, and impedance performance were also investigated. As the content of graphene increased, the percolation phenomenon appeared and the conductive mechanism of the resulting composites changed. Interestingly, a negative permittivity conforming to Drude model was also observed. Further investigation revealed that there is a corresponding relationship between the permittivity and the reactance from the perspective of a microcircuit.

2. EXPERIMENTAL SECTION

2.1. Materials and Fabrication. In this work, the flaky graphene powders (purity ∼99.7%, average thickness is 4−7 nm and average diameter is ∼80 μm) were purchased from Nanjing JCNANO Technology Co., Ltd. (China). The Sylgard 184 silicone elastomer kit (Dow Corning Company, USA) including the silicone elastomer base (Sylgard 184A) and curing agent (Sylgard 184B) was used to prepare the flexible PDMS matrix. The normal heptane (*n*-heptane, purity ∼99.9%) solvent was purchased from Thermo Fisher Scientific Co., Ltd. (China). All materials are used directly without any further treatment. The flexible GR/PDMS metacomposites were fabricated by an in situ polymerization method. The detailed preparation process was described as follows.

The silicone elastomer base, curing agent, and *n*-heptane were mixed in the beaker with a mass radio of 10:1:10 and stirred for 10 min using a magnetic stirrer. Subsequently, the graphene sheets with different mass ratios (0, 1, 2, 3, and 4 wt %, respectively) were weighed and added into the aforementioned mixture. In order to avoid the agglomeration of graphene and improve the dispersion of mixture, the slurry was ultrasonically treated and stirred repeatedly at room temperature (RT). After the flaky graphene powders were uniformly and thoroughly dispersed in the polymer matrix, the mixed suspension was poured into a rubber mold at a constant speed. Then the mold of the mixed suspension was put into a vacuum drying oven and cured at 393 K for 100 min. After that, the flexible matrix PDMS was totally cured, and the GR/PDMS composites were successfully fabricated.

2.2. Characterizations and Measurements. The microstructure of the resulting composites was observed by field emission scanning electron microscope (FESEM; Zeiss Sigma 500, Germany). The phase analysis of samples was detected by X-ray diffraction (XRD; PANalytical X'Pert PRO, The Netherlands), and the diffraction angle was in the range of $10° < 2\theta < 90°$. The Fourier transform infrared (FT-IR) spectra of the samples in the range of 500−4000 cm^{-1} were obtained by FT-IR spectroscopy (Thermo Scientific Nicolet IS 10, USA) at a resolution of 4 cm^{-1}. The Raman spectra in the range of 1200−2800 cm^{-1} were measured by a Raman microscope (Renishaw Invia, U.K.) equipped with a 514 nm laser excitation.

The permittivity spectra of the GR/PDMS composites were measured by a parallel plate method using a LCR meter (Keysight E4980AL, USA) from 20 Hz to 1 MHz. Platinum films were sputtered on both sides of the samples to reduce the measurement error derived from the air gap. The upper electrode was processed into annulus to eliminate the stray capacitance derived from the edge of the sample. Before testing, the stray admittance and residual impedances of the test fixtures should be eliminated by the open and short compensation, respectively. After that, the electrodes were adjusted to be in parallel, and then the samples contacted the two electrodes for measurement. The permittivity and ac conductivity can be calculated using the measured capacitance C and resistance R, which can be described as follows,

$$\varepsilon_r' = \frac{tC}{A\varepsilon_0} \tag{1}$$

$$\sigma_{ac} = \frac{t}{RA} \tag{2}$$

where the ε_r' and σ_{ac} are permittivity, ac is conductivity, and t, A, R, and C are the thickness of the sample, the area of the electrode, the measured resistance, and capacitance, respectively, and ε_0 is the permittivity of vacuum (8.85×10^{-12} F/m).

DOI: 10.1021/acs.jpcc.9b06753
J. Phys. Chem. C 2019, 123, 23635−23642

3. RESULTS AND DISCUSSION

The FT-IR spectra of GR/PDMS metacomposites with different content of graphene are shown in Figure 1. For the

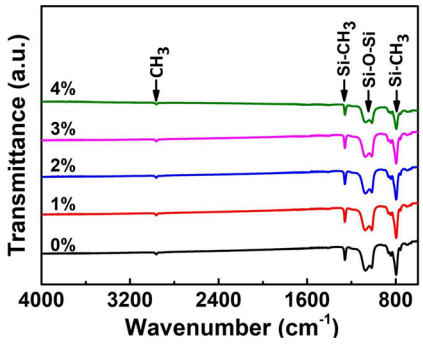

Figure 1. FT-IR spectra of GR/PDMS composites with different graphene content (0–4 wt %).

pure PDMS, a telescopic vibration peak appeared at about 790 cm^{-1}, which resulted from the in-plane bending or scissoring of the $Si-CH_3$ bond. Meanwhile, when the wavenumber was located at about 1259 cm^{-1}, a deformation vibration peak was observed mainly due to the out-of-plane oscillations of the $Si-CH_3$ bond.[45] In addition, the twin-peak was observed at about 1100 and 1020 cm^{-1}, which was attributed to the asymmetric and symmetric stretching vibration of the two neighbor siloxane bonds (shown as Si–O–Si).[46] At about 2960 cm^{-1}, a telescopic vibration peak corresponding to the methyl was observed, which was associated with the asymmetric stretching vibration. Compared with that of pure PDMS, the characteristic peaks in GR/PDMS composites were also observed at the corresponding position, which indicated that there was no reaction between PDMS and graphene during the synthesis process.

Figure 2 shows the Raman spectra of GR/PDMS composites with different graphene loadings. As is well-known, the Raman

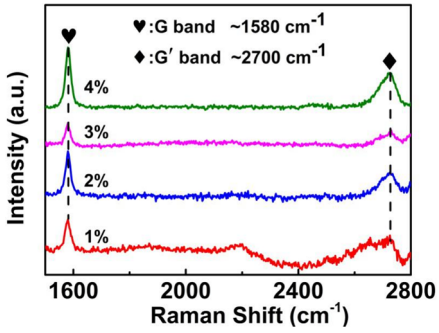

Figure 2. Raman spectra of GR/PDMS composites with different graphene loadings.

spectrum of graphene consists of several bands, mainly including three characteristic bands: D band, G band, and G′ band (also called 2D band). A distinct G band was observed at ~1580 cm^{-1} in GR/PDMS composites, and the intensity of the G band gradually increased with the increase of graphene. The G band was determined by the internal vibrations of the sp^2 carbon atom and was associated with highly ordered graphite. Meanwhile, the G′ band originating from a double resonance process appeared at ~2700 cm^{-1}, which reflected the characteristic of few-layer graphene. In GR/PDMS composites, the G′ band was wider and lower than that of G band. Moreover, the D band was not distinct in these Raman spectra. The very weak D band intensity indicated that the edge defects of the selected graphene were very few.[47] With the increase of graphene, there was no shift for the G band and G′ band in the composites (shown as the dotted lines), indicating that the PDMS has no effect on the microstructure of graphene during the polymerization process.

The XRD patterns and SEM images of GR/PDMS composites are presented in Figure 3. As shown in Figure 3a, the amorphous structure with a wide peak appeared at about 12°, which was related to the minicrystal diffraction of PDMS. When graphene was incorporated into the matrix, the characteristic peak was observed at about 26.5°, indicating a high graphitization. As graphene content increased, the peak of graphene in the resulting composites still remained at the corresponding position. Meanwhile, the diffraction intensity of graphene was gradually enhanced. Figure 3b presented the microstructure of pure graphene with a laminate structure. The microstructures of GR/PDMS composites were shown in Figure 3c–f. When graphene sheets were at a low loading level, they were randomly distributed in PDMS matrix. The inset in Figure 3c is the partial enlarged view of the microstructure, which exhibited that the flaky graphene got together and was surrounded by the matrix. Therefore, graphene sheets were hardly to be observed from the surface of the resulting composites. With the increase of graphene, the graphene sheets gradually connected with each other and formed a network. As shown in Figure 3e, the PDMS (bright) and the graphene (dark) were uniformly distributed and matched well. It can be seen that the isolated graphene sheets eventually established a three-dimensional network throughout the composites. With further increasing of the graphene content, the connectivity among the graphene sheets got enhanced (Figure 3f). Moreover, the GR/PDMS composites with high graphene content (4 wt %) still maintained excellent flexibility, as shown in the inset of Figure 3f. It is well-known that the physical properties of the composites will undergo an abrupt transition along with the percolation phenomenon of microstructure.[48] Therefore, the electrical conductivity and permittivity are further studied as follows.

Figure 4 shows the ac conductivity σ_{ac} spectra of GR/PDMS composites with different mass ratios of graphene. At the outset of test frequency, the conductivity of the resulting composites got enhanced with the increase of graphene. For the samples with lower content of graphene, the trend of σ_{ac} went up as the frequency increased. The variation trend signified that the electrical conductivity spectra obeyed Jonscher's power law.[49] As shown in Figure 4, the measured results were in good agreement with the fitted data, which conformed to the power law. Although some graphene sheets got together and formed clusters, the conductive network can be hardly established when the content of graphene was at a low level. Hence, the electrons in GR/PDMS composites migrated in the formation of discontinuous hopping. It is manifested that the electrons can gain more energy in high frequency, thereby contributing to their hopping conduction, which leads to the increase of electric conductivity. After GR/PDMS composites reached a percolating state, the conductivity was gradually decreased in a higher frequency region due to the skin effect.[25] As shown in Figure 3, a continuous network was eventually constructed when the content of graphene reached 3 wt %, so the electrons can make a long-range motion

DOI: 10.1021/acs.jpcc.9b06753
J. Phys. Chem. C 2019, 123, 23635–23642

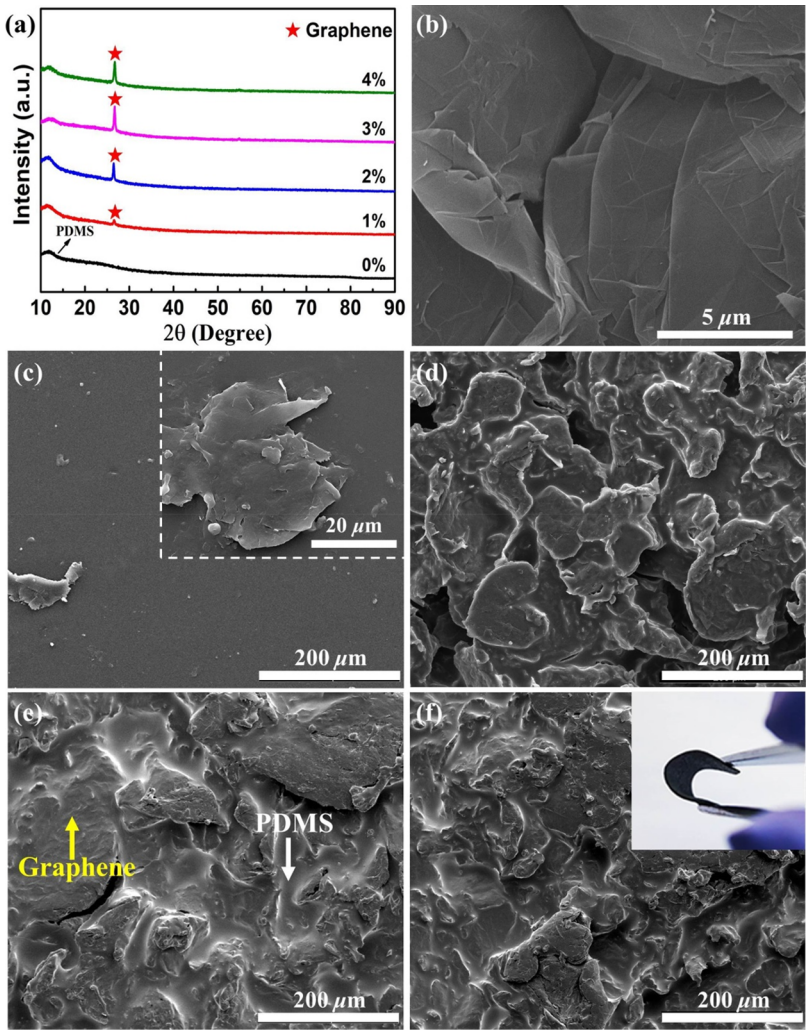

Figure 3. XRD patterns (a) and SEM images (b–f) of GR/PDMS composites with 0, 1, 2, 3, and 4 wt % graphene. The inset in (c) is the partial enlarged view and the inset in (f) shows the good flexibility of GR/PDMS composites with 4 wt % graphene.

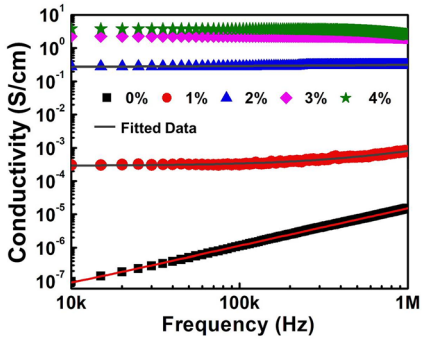

Figure 4. The ac conductivity spectra of GR/PDMS composites. The solid lines in (b) show the fitted results based on the Jonscher's power law.

along the conductive pathways and the resulting composites exhibited a conduction behavior. That is, the conductive mechanism of the resulting composites changes from hopping conduction to electron conduction with the increase of graphene. A similar phenomenon was also observed in $CaCu_3Ti_4O_{12}$ ceramic-based composites with carbon materials.[50]

The permittivity spectra of GR/PDMS composites are shown in Figure 5. The dielectric constant of pure PDMS was very small and weakly dependent on frequency. When the conductive graphene was incorporated into the insulating PDMS matrix, the space charges surrounded the interfaces between graphene and PDMS and gave rise to the enhancement of interfacial polarization, which played a dominant role in the polarization of the dipoles. As is well-known, the dielectric property of a medium was attributed to its polarizability, so the dielectric constant of the resulting composites was remarkably increased compared with that of pristine PDMS (Figure 5a). This phenomenon was also called Maxwell–Wagner–Sillars effect,[51] which was widespread in the conductor–insulator composites. With further increasing of the content of graphene, the permittivity of GR/PDMS composites measured at the outset of test frequency region can reach about 100. As mentioned above, the conductive mechanism underwent an abrupt transition along with the percolation phenomenon of microstructure. Interestingly, the permittivity converted from positive to negative (Figure 5b), when GR/PDMS composites reached a percolating state. Under the action of an external electric field, the negative permittivity of GR/PDMS composites conformed to the

DOI: 10.1021/acs.jpcc.9b06753
J. Phys. Chem. C 2019, 123, 23635–23642

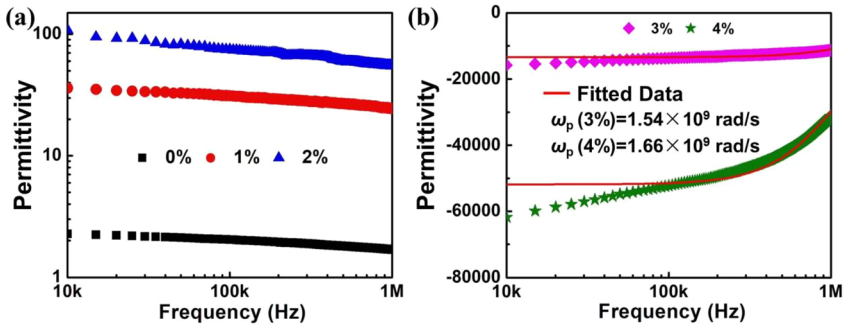

Figure 5. Permittivity spectra of GR/PDMS composites. (a) and (b) show the positive and negative permittivity spectra, respectively. The solid lines in (b) show the fitted results based on the Drude model.

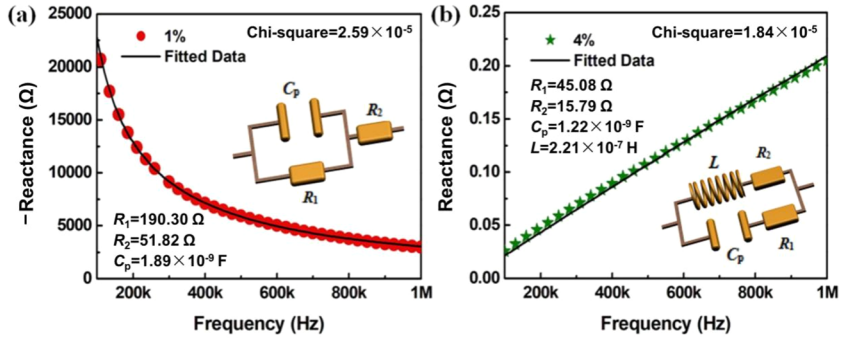

Figure 6. Dependence of reactance on frequency for GR/PDMS composites. (a) and (b) are the reactance spectra of GR/PDMS composites below and above the percolation threshold, respectively. The insets show the equivalent circuits.

Drude model, which can be described by the following equation,[19]

$$\varepsilon_r'(\omega) = 1 - \frac{{\omega_p}^2}{\omega^2 + {\omega_\tau}^2} \tag{3}$$

$$\omega_p = \sqrt{\frac{ne^2}{m\varepsilon_0}} \tag{4}$$

where ω is the test angular frequency, ω_p is the plasma angular frequency, ω_τ is the collision frequency (the inverse relaxation time $1/\tau$), m is the effective mass, n is the effective electron density, ε_0 is the vacuum permittivity, and e is the electron charge (1.6×10^{-19} C).

The electrons can generate a collective harmonic oscillation under the action of an alternating electric field due to the restoring force from the separation of positive and negative charges, which is also called plasma oscillation. For pure metal materials, the negative permittivity can be observed below the plasma oscillation frequency. As is well-known, the electron density in pure metals is ultrahigh, so their plasma oscillation frequency of pure metals is commonly located in the visible or near-ultraviolet region.[52] Especially in the radio frequency region, the absolute values of the negative permittivity are very huge (usually 10^5−10^6), while the dissipation is much greater,[53] indicating that the complex permittivity is essentially imaginary.

For metal materials, their two-dimensional plasmon behavior follows the relationship $\omega_p \propto n^{1/2}$ (n is the electron density). For graphene, the relationship between plasma oscillation frequency and electron density follows $\omega_p \propto n^{1/4}$,[54] which is ascribed to its unique electronic energy dispersion and band structure.[55] On the other hand, carbon materials possess much lower intrinsic electron density. When graphene is embedded in the insulating matrix, their electron density was further diluted. Therefore, compared with those of metal materials, the plasma oscillation frequency of GR/PDMS composites is dramatically reduced to the microwave frequency region. Meanwhile, the absolute values of GR/PDMS composites remarkably decreased compared with those of metal materials. In order to further clarify the internal mechanism of negative permittivity from the view of microelectronics, the relationship between the permittivity and the reactance was studied according to the equivalent circuit analysis in the following section.

Figure 6 shows the reactance spectra of GR/PDMS composites with positive and negative permittivity, respectively. For the composites with positive permittivity behavior, the reactance was negative in the overall test frequency range (Figure 6a). It means that the voltage phase falls behind the current phase, indicating a capacitive character. As is well-known, the capacitive reactance is inversely proportional to the test frequency, so the absolute values of the reactance gradually decreased with the increment of frequency. When graphene content was above the percolation threshold, the positive reactance is proportional to the frequency of electric field (Figure 6b), indicating an inductive character.

In order to verify the reactance character as mentioned above, the equivalent circuit analysis was performed by the ZSimpwin software.[10] The optimal equivalent circuit was determined by the χ^2 value, which signifies the precision of the selected equivalent circuit model. The fitted results are shown in Figure 6, and the χ^2 values are very small, which indicates that the fitted data are in good accordance with the measured results. In the sample with positive permittivity, the circuit was composed of resistors and capacitor (shown in the inset of

DOI: 10.1021/acs.jpcc.9b06753
J. Phys. Chem. C 2019, 123, 23635−23642

Figure 6a). The interfaces between graphene and the insulating PDMS can be regarded as amounts of microcapacitors. The resistors come from the contact resistance and the interface resistance.[20] When graphene content was far less than the percolation threshold, the dipoles played a primary role in the composites and the composites presented a capacitive character. Interestingly, the particular inductor occurred when the connected graphene sheets formed a percolation network. The circuit of the percolating composites consisted of inductor as well as resistor and capacitor (shown in the inset of Figure 6b). The conduction electrons can migrate around the interconnected graphene network and form a closed loop, leading to the formation of an inductor. On the other hand, the graphene clusters dispersed to the matrix can generate polarized electrons, which are responsible for the capacitor.

Further study indicated that the permittivity and the reactance satisfy a corresponding relationship, which can be described as follows.[56]

$$\varepsilon_r' = -\frac{Z''}{2f\pi C_0(Z'^2 + Z''^2)} \quad (5)$$

where ε_r' is the permittivity, Z' and Z'' are the resistance and reactance, f is the test frequency, and C_0 is the capacitance of vacuum. It signified that the permittivity is determined by the reactance. When the reactance is negative, the permittivity is positive and the composites possess capacitive character. On the contrary, when the reactance is positive, it leads to negative permittivity, and the inductive character played an overwhelming role in the microcircuit. Therefore, the capacitive character is responsible for the positive permittivity, and the inductive character contributes to negative permittivity.

4. CONCLUSIONS

In this paper, the flexible GR/PDMS metacomposites with different graphene mass ratios (0−4 wt %) were fabricated via an in situ polymerization method. It is manifested that the conduction mechanism of the resulting composites changed from hopping conduction to electron conduction, along with the formation of percolating network. Moreover, when graphene content was below 3 wt %, the permittivity became enhanced with the increase of graphene due largely to the Maxwell−Wagner−Sillars effect. Interestingly, the Drude-like negative permittivity was observed in the composites, when graphene reached a percolating state. After embedding of graphene into the insulating matrix, the electrons of the resulting composites were diluted and gave rise to a low frequency plasmonic state. Further investigation revealed that there is a corresponding relationship between the permittivity and the reactance. Specifically, the negative permittivity was attributed to the inductive character deriving from the conductive network, while the positive permittivity was dependent on the capacitive character. Hopefully, the flexible metacomposites with tunable negative permittivity is of great significance in flexible electronic devices, wearable cloaks, stretchable sensors, and thin-film capacitors.

AUTHOR INFORMATION

Corresponding Authors

*Q.H.: e-mail, qing.hou.16@ucl.ac.uk.
*R.F.: e-mail, rhfan@shmtu.edu.cn.
*Z.G.: e-mail, zguo10@utk.edu.

ORCID

Kai Sun: 0000-0001-7396-5813
Zhanhu Guo: 0000-0003-0134-0210

Notes

The authors declare no competing financial interest.

ACKNOWLEDGMENTS

The authors acknowledge the financial support from National Natural Science Foundation of China (Grants 51803119, 51871146, and 51701115), the Innovation Program of Shanghai Municipal Education Commission (Grant 2019-01-07-00-10-E00053), "Chenguang Program" supported by Shanghai Education Development Foundation and Shanghai Municipal Education Commission (Grant 18CG56), China Postdoctoral Science Foundation (Grant 2017M611757), and the Science and Technology Commission of Shanghai Municipality (Grant 18DZ1112902).

REFERENCES

(1) Khan, A. I.; Bhowmik, D.; Yu, P.; Kim, S. J.; Pan, X.; Ramesh, R.; Salahuddin, S. Experimental Evidence of Ferroelectric Negative Capacitance in Nanoscale Heterostructures. *Appl. Phys. Lett.* **2011**, *99*, 113501.

(2) Khan, A. I.; Chatterjee, K.; Wang, B.; Drapcho, S.; You, L.; Serrao, C.; Bakaul, S. R.; Ramesh, R.; Salahuddin, S. Negative Capacitance in a Ferroelectric Capacitor. *Nat. Mater.* **2015**, *14*, 182.

(3) Shi, Z.; Wang, J.; Mao, F.; Yang, C.; Zhang, C.; Fan, R. Significantly Improved Dielectric Performances of Sandwich-Structured Polymer Composites Induced by Alternating Positive-*k* and Negative-*k* Layers. *J. Mater. Chem. A* **2017**, *5*, 14575−14582.

(4) Liu, C.; Behdad, N. High-Power Microwave Filters and Frequency Selective Surfaces Exploiting Electromagnetic Wave Tunneling through *ε*-Negative Layers. *J. Appl. Phys.* **2013**, *113*, 064909.

(5) Kim, H.; Hopwood, J. Wave Propagation in Composites of Plasma and Metamaterials with Negative Permittivity and Permeability. *Sci. Rep.* **2019**, *9*, 3024.

(6) Schurig, D.; Mock, J.; Smith, D. Electric-Field-Coupled Resonators for Negative Permittivity Metamaterials. *Appl. Phys. Lett.* **2006**, *88*, 041109.

(7) Shalaev, V. M. Optical Negative-Index Metamaterials. *Nat. Photonics* **2007**, *1*, 41.

(8) Sun, K.; Fan, R.; Zhang, X.; Zhang, Z.; Shi, Z.; Wang, N.; Xie, P.; Wang, Z.; Fan, G.; Liu, H.; et al. An Overview of Metamaterials and Their Achievements in Wireless Power Transfer. *J. Mater. Chem. C* **2018**, *6*, 2925−2943.

(9) Huang, X.; Yin, R.; Qian, L.; Zhao, W.; Liu, H.; Liu, C.; Fan, J.; Hou, H.; Zhang, J.; Guo, Z. Processing Conditions Dependent Tunable Negative Permittivity in Reduced Graphene Oxide-Alumina Nanocomposites. *Ceram. Int.* **2019**, *45*, 17784−17792.

(10) Xie, P.; Wang, Z.; Zhang, Z.; Fan, R.; Cheng, C.; Liu, H.; Liu, Y.; Li, T.; Yan, C.; Wang, N.; Guo, Z. Silica Microspheres Templated Self-Assembly of Three-Dimensional Carbon Network with Stable Radio-Frequency Negative Permittivity and Low Dielectric loss. *J. Mater. Chem. C* **2018**, *6*, 5239−5249.

(11) Zhao, B.; Park, C. B. Tunable Electromagnetic Shielding Properties of Conductive Poly (Vinylidene Fluoride)/Ni Chain Composite Films with Negative Permittivity. *J. Mater. Chem. C* **2017**, *5*, 6954−6961.

(12) Zhu, J.; Wei, S.; Zhang, L.; Mao, Y.; Ryu, J.; Karki, A. B.; Young, D. P.; Guo, Z. Polyaniline-Tungsten Oxide Metacomposites with Tunable Electronic Properties. *J. Mater. Chem.* **2011**, *21*, 342−348.

(13) Chen, H. Metamaterials: Constitutive Parameters, Performance, and Chemical Methods for Realization. *J. Mater. Chem.* **2011**, *21*, 6452−6463.

DOI: 10.1021/acs.jpcc.9b06753
J. Phys. Chem. C 2019, 123, 23635−23642

(14) Cheng, C.; Fan, R.; Fan, G.; Liu, H.; Zhang, J.; Shen, J.; Ma, Q.; Wei, R.; Guo, Z. Tunable Negative Permittivity and Magnetic Performance of Yttrium Iron Garnet/Polypyrrole Metacomposites at the RF Frequency. *J. Mater. Chem. C* **2019**, *7*, 3160−3167.
(15) Shi, Z.; Fan, R.; Yan, K.; Sun, K.; Zhang, M.; Wang, C.; Liu, X.; Zhang, X. Preparation of Iron Networks Hosted in Porous Alumina with Tunable Negative Permittivity and Permeability. *Adv. Funct. Mater.* **2013**, *23*, 4123−4132.
(16) Tsutaoka, T.; Massango, H.; Kasagi, T.; Yamamoto, S.; Hatakeyama, K. Double Negative Electromagnetic Properties of Percolated $Fe_{53}Ni_{47}$/Cu Granular Composites. *Appl. Phys. Lett.* **2016**, *108*, 191904.
(17) Yao, X.; Kou, X.; Qiu, J. Multi-Walled Carbon Nanotubes/Polyaniline Composites with Negative Permittivity and Negative Permeability. *Carbon* **2016**, *107*, 261−267.
(18) Yin, R.; Wu, H.; Sun, K.; Li, X.; Yan, C.; Zhao, W.; Guo, Z.; Qian, L. Fabrication of Graphene Network in Alumina Ceramics with Adjustable Negative Permittivity by Spark Plasma Sintering. *J. Phys. Chem. C* **2018**, *122*, 1791−1799.
(19) Yan, K.; Fan, R.; Shi, Z.; Chen, M.; Qian, L.; Wei, Y.; Sun, K.; Li, J. Negative Permittivity Behavior and Magnetic Performance of Perovskite $La_{1-x}Sr_xMnO_3$ at High-Frequency. *J. Mater. Chem. C* **2014**, *2*, 1028−1033.
(20) Xie, P.; Sun, K.; Wang, Z.; Liu, Y.; Fan, R.; Zhang, Z.; Schumacher, G. Negative Permittivity Adjusted by SiO_2-Coated Metallic Particles in Percolative Composites. *J. Alloys Compd.* **2017**, *725*, 1259−1263.
(21) Sun, K.; Xin, J.; Li, Y.; Wang, Z.; Hou, Q.; Li, X.; Wu, X.; Fan, R.; Choy, K. L. Negative Permittivity Derived from Inductive Characteristic in the Percolating Cu/Ep Metacomposites. *J. Mater. Sci. Technol.* **2019**, DOI: 10.1016/j.jmst.2019.07.015.
(22) Sun, K.; Xin, J.; Wang, Z.; Feng, S.; Wang, Z.; Fan, R.; Liu, H.; Guo, Z. Weakly Negative Permittivity and Low Frequency Dispersive Behavior in Graphene/Epoxy Metacomposites. *J. Mater. Sci.: Mater. Electron.* **2019**, *30*, 14745−14754.
(23) Wang, J.; Shi, Z.; Mao, F.; Chen, S.; Wang, X. Bilayer Polymer Metacomposites Containing Negative Permittivity Layer for New High-*k* Materials. *ACS Appl. Mater. Interfaces* **2017**, *9*, 1793−1800.
(24) Shi, Z.; Fan, R.; Zhang, Z.; Qian, L.; Gao, M.; Zhang, M.; Zheng, L.; Zhang, X.; Yin, L. Random Composites of Nickel Networks Supported by Porous Alumina toward Double Negative Materials. *Adv. Mater.* **2012**, *24*, 2349−2352.
(25) Sun, K.; Fan, R.; Zhang, Z.; Yan, K.; Zhang, X.; Xie, P.; Yu, M.; Pan, S. The Tunable Negative Permittivity and Negative Permeability of Percolative Fe/Al_2O_3 Composites in Radio Frequency Range. *Appl. Phys. Lett.* **2015**, *106*, 172902.
(26) Shi, Z.; Fan, R.; Zhang, Z.; Gong, H.; Ouyang, J.; Bai, Y.; Zhang, X.; Yin, L. Experimental and Theoretical Investigation on the High Frequency Dielectric Properties of Ag/Al_2O_3 Composites. *Appl. Phys. Lett.* **2011**, *99*, 032903.
(27) Sun, K.; Zhang, Z.; Qian, L.; Dang, F.; Zhang, X.; Fan, R. Dual Percolation Behaviors of Electrical and Thermal Conductivity in Metal-Ceramic Composites. *Appl. Phys. Lett.* **2016**, *108*, 061903.
(28) Chen, M.; Fan, R.; Gao, M.; Pan, S.; Yu, M.; Zhang, Z. Negative Permittivity Behavior in $Fe_{50}Ni_{50}/Al_2O_3$ Magnetic Composite near Percolation Threshold. *J. Magn. Magn. Mater.* **2015**, *381*, 105−108.
(29) Tsutaoka, T.; Kasagi, T.; Yamamoto, S.; Hatakeyama, K. Low Frequency Plasmonic State and Negative Permittivity Spectra of Coagulated Cu Granular Composite Materials in the Percolation Threshold. *Appl. Phys. Lett.* **2013**, *102*, 181904.
(30) Yao, X.; Kou, X.; Qiu, J.; Moloney, M. Generation Mechanism of Negative Dielectric Properties of Metallic Oxide Crystals/Polyaniline Composites. *J. Phys. Chem. C* **2016**, *120*, 4937−4944.
(31) Gu, H.; Xu, X.; Dong, M.; Xie, P.; Shao, Q.; Fan, R.; Liu, C.; Wu, S.; Wei, R.; Guo, Z. Carbon Nanospheres Induced High Negative Permittivity in Nanosilver-Polydopamine Metacomposites. *Carbon* **2019**, *147*, 550−558.
(32) Zhu, J.; Wei, S.; Zhang, L.; Mao, Y.; Ryu, J.; Mavinakuli, P.; Karki, A. B.; Young, D. P.; Guo, Z. Conductive Polypyrrole/Tungsten Oxide Metacomposites with Negative Permittivity. *J. Phys. Chem. C* **2010**, *114*, 16335−16342.
(33) Boltasseva, A.; Atwater, H. A. Low-Loss Plasmonic Metamaterials. *Science* **2011**, *331*, 290−291.
(34) Cheng, C.; Fan, R.; Ren, Y.; Ding, T.; Qian, L.; Guo, J.; Li, X.; An, L.; Lei, Y.; Yin, Y.; Guo, Z. Radio Frequency Negative Permittivity in Random Carbon Nanotubes/Alumina Nanocomposites. *Nanoscale* **2017**, *9*, 5779−5787.
(35) Le, K.; Wang, Z.; Wang, F.; Wang, Q.; Shao, Q.; Murugadoss, V.; Wu, S.; Liu, W.; Liu, J.; Gao, Q.; Guo, Z. Sandwich-Like NiCo Layered Double Hydroxides/Reduced Graphene Oxide Nanocomposite Cathode for High Energy Density Asymmetric Supercapacitors. *Dalton T.* **2019**, *48*, 5193−5202.
(36) Cheng, C.; Fan, R.; Wang, Z.; Xie, P.; Hou, C.; Fan, G.; Lei, Y.; An, L.; Liu, Y. Radio-Frequency Negative Permittivity in the Graphene/Silicon Nitride Composites Prepared by Spark Plasma Sintering. *J. Am. Ceram. Soc.* **2018**, *101*, 1598−1606.
(37) Yang, S.; Liu, P.; Yang, M.; Wang, Q.; Song, J.; Dong, L. From Flexible and Stretchable Meta-Atom to Metamaterial: A Wearable Microwave Meta-Skin with Tunable Frequency Selective and Cloaking Effects. *Sci. Rep.* **2016**, *6*, 21921.
(38) Zhu, J.; Wei, S.; Ryu, J.; Guo, Z. Strain-Sensing Elastomer/Carbon Nanofiber "Metacomposites". *J. Phys. Chem. C* **2011**, *115*, 13215−13222.
(39) Zhang, C.; Shi, Z.; Mao, F.; Yang, C.; Zhu, X.; Yang, J.; Zuo, H.; Fan, R. Flexible Polyimide Nanocomposites with Dc Bias Induced Excellent Dielectric Tunability and Unique Nonpercolative Negative-*k* toward Intrinsic Metamaterials. *ACS Appl. Mater. Interfaces* **2018**, *10*, 26713−26722.
(40) Allen, M. J.; Tung, V. C.; Kaner, R. B. Honeycomb Carbon: A Review of Graphene. *Chem. Rev.* **2010**, *110*, 132−145.
(41) Mates, J. E.; Bayer, I. S.; Palumbo, J. M.; Carroll, P. J.; Megaridis, C. M. Extremely Stretchable and Conductive Water-Repellent Coatings for Low-Cost Ultra-Flexible Electronics. *Nat. Commun.* **2015**, *6*, 8874.
(42) Yamada, T.; Hayamizu, Y.; Yamamoto, Y.; Yomogida, Y.; Izadi-Najafabadi, A.; Futaba, D. N.; Hata, K. A Stretchable Carbon Nanotube Strain Sensor for Human-Motion Detection. *Nat. Nanotechnol.* **2011**, *6*, 296.
(43) Yao, H. B.; Ge, J.; Wang, C. F.; Wang, X.; Hu, W.; Zheng, Z. J.; Ni, Y.; Yu, S. H. A Flexible and Highly Pressure-Sensitive Graphene−Polyurethane Sponge Based on Fractured Microstructure Design. *Adv. Mater.* **2013**, *25*, 6692−6698.
(44) Sun, K.; Xie, P.; Wang, Z.; Su, T.; Shao, Q.; Ryu, J.; Zhang, X.; Guo, J.; Shankar, A.; Li, J.; et al. Flexible Polydimethylsiloxane/Multi-Walled Carbon Nanotubes Membranous Metacomposites with Negative Permittivity. *Polymer* **2017**, *125*, 50−57.
(45) Wang, L.; Ji, Q.; Glass, T.; Ward, T.; McGrath, J.; Muggli, M.; Burns, G.; Sorathia, U. Synthesis and Characterization of Organosiloxane Modified Segmented Polyether Polyurethanes. *Polymer* **2000**, *41*, 5083−5093.
(46) Chazalviel, J. N.; Rodrigues-Filho, U. P. On the Nsio Infrared Absorption of Polysiloxane Films. *Thin Solid Films* **2012**, *520*, 3918−3921.
(47) Malard, L.; Pimenta, M.; Dresselhaus, G.; Dresselhaus, M. Raman Spectroscopy in Graphene. *Phys. Rep.* **2009**, *473*, 51−87.
(48) Sun, K.; Fan, R.; Yin, Y.; Guo, J.; Li, X.; Lei, Y.; An, L.; Cheng, C.; Guo, Z. Tunable Negative Permittivity with Fano-Like Resonance and Magnetic Property in Percolative Silver/Yittrium Iron Garnet Nanocomposites. *J. Phys. Chem. C* **2017**, *121*, 7564−7571.
(49) Dong, J.; Wang, Z.; Sun, K.; Jiang, Q.; Xie, P.; Fan, G.; Qu, Y.; An, L.; Fan, R. Flexible Acrylic-Polyurethane/Copper Composites with a Frequency and Temperature-Independent Permittivity. *J. Mater. Sci.: Mater. Electron.* **2018**, *29*, 20832−20839.
(50) Qu, Y.; Fan, G.; Liu, D.; Gao, Y.; Xu, C.; Zhong, J.; Xie, P.; Liu, Y.; Wu, Y.; Fan, R. Functional Nano-Units Prepared by Electrostatic Self-Assembly for Three-Dimension Carbon Networks Hosted in

DOI: 10.1021/acs.jpcc.9b06753
J. Phys. Chem. C 2019, 123, 23635−23642

$CaCu_3Ti_4O_{12}$ Ceramics Towards Radio-Frequency Negative Permittivity. *J. Alloys Compd.* **2018**, *743*, 618−625.
(51) Yousefi, N.; Sun, X.; Lin, X.; Shen, X.; Jia, J.; Zhang, B.; Tang, B.; Chan, M.; Kim, J. K. Highly Aligned Graphene/Polymer Nanocomposites with Excellent Dielectric Properties for High-Performance Electromagnetic Interference Shielding. *Adv. Mater.* **2014**, *26*, 5480−5487.
(52) Gao, M.; Shi, Z.; Fan, R.; Qian, L.; Zhang, Z.; Guo, J. High-Frequency Negative Permittivity from Fe/Al_2O_3 Composites with High Metal Contents. *J. Am. Ceram. Soc.* **2012**, *95*, 67−70.
(53) Pendry, J. B. Negative Refraction Makes a Perfect Lens. *Phys. Rev. Lett.* **2000**, *85*, 3966.
(54) Hwang, E.; Sarma, S. D. Dielectric Function, Screening, and Plasmons in Two-Dimensional Graphene. *Phys. Rev. B: Condens. Matter Mater. Phys.* **2007**, *75*, 205418.
(55) Zhu, J.; Luo, Z.; Wu, S.; Haldolaarachchige, N.; Young, D. P.; Wei, S.; Guo, Z. Magnetic Graphene Nanocomposites: Electron Conduction, Giant Magnetoresistance and Tunable Negative Permittivity. *J. Mater. Chem.* **2012**, *22*, 835−844.
(56) Sharma, S.; Basu, T.; Shahee, A.; Singh, K.; Lalla, N.; Sampathkumaran, E. Complex Dielectric and Impedance Behavior of Magnetoelectric Fe_2TiO_5. *J. Alloys Compd.* **2016**, *663*, 289−294.

DOI: 10.1021/acs.jpcc.9b06753
J. Phys. Chem. C 2019, 123, 23635−23642